CARMA Memorandum Series #15

# CARMA Configurations for Cedar Flat Using a 5-Arm Star Array

Glen R. Petitpas
*University of Maryland*
*College Park MD, USA 20742*
petitpas@astro.umd.edu
and
Lee G. Mundy
*University of Maryland*
*College Park MD, USA 20742*
lgm@astro.umd.edu

September 29, 2003

**ABSTRACT**

We present 5-arm star configurations for the CARMA array and compare with the "optimized" configurations proposed by Helfer & Wright (2003) and Helfer (2003). The 5-arm star provides similar performance to the purely "optimized" array while reducing environmental impacts by reducing the number of roads that need to be created. It simplifies construction of roads and cable trenches because of its five straight arms. It also provides modest construction and operational cost savings by allowing more efficient reuse of antenna pads between arrays (53 compared to 60 for the "optimized" array). We are capable of re-creating (within realistic operational parameters) comparable beam and sidelobe performance as the fully optimized array. Unfortunately the rigid geometric shape makes it less adaptable to the asymetric Cedar Flat geography.

## 1. Introduction

The Boone (2001) code is an excellent tool for generating arrays with acceptable beam properties and good UV coverage. It does have some major drawbacks. The first is that it lays antennas anywhere it needs. To simplify the problem of running cables and roads to all of the dishes, we have generated a series of configurations that all (except a few A-array pads) lie along the arms of a 5-arm star. The benefit is that with almost all antennas along five roads, there are fewer roads to build, which reduces costs. This has the added advantage of saving on operational costs after construction such as road resurfacing, snow-ploughing, etc. Also simplified is the problem of running underground cables to each pad. The terrain at Cedar Flat is very rocky in many places, and running cables to each pad will present problems in the best case scenario.

Additionally, future hybrid configurations will be easier to incorporate into the existing road, cable, and pad structure. There is greater oppotunity for pad reuse since we are limited in where we get to place dishes from configuration to configuration. Although the current configurations do not force large amounts of pad reuse, we still populate all five configurations with just 50 antenna pads.

## 2. The Configurations

We have modified the existing site "mask" used by Helfer & Wright (2003) to overlay a five arm star with arms of width 10 m (see Figure 1). We have also used the Boone optimization code, but optimized for source declinations of 15° to ensure that the beams are rounder at the elevations where atmospheric opacity is best. Since ALMA will dominate observations of the southern sky when it arrives, it seems prudent to optimize for the northern part of the sky where CARMA will remain the domininant mm array. Helfer & Wright (2003) choose to optimize for the special case of 0° declination. We feel that the slight decrease in performance at 0.0° is more than made up for by the better beams at higher declinations.

The arrays presented below have a maximum baseline of 1.8 km which results in a synthesized beam of $0.14 \times 0.14''$ at $+30°$ declination (see Table 1). For the E-array, we obain a resolution of $\sim 4''$, but it more likely that we will adopt the E-array from Helfer & Wright (2003) since it is basically as tight as you can pack the 15 dishes together and has superior shadowing properties. Our resulting configurations have a factor of approximately 2.0-2.5 in resolution between each configuration. The downside of this is the large jump in brightness temperature sensitivity between A- and B-arrays. If needed, a hybrid array could be easily generated from the existing pads, but presumably this will be compensated for by the standard practice of simply combining data from A- and B-arrays.

### 2.1. Details and Techniques

Our arrays are shown in Figure 2. The resulting beams are shown in Figure 3 and 4. For completeness our *uv* coverage and *uv* density vs baseline plots are shown in Figures 5 and 6 respectively.

Initially, the C-array was optimized within the star mask and a target resolution of just under $1''$ (at 230 GHz) was set. Once this array was created, six of the inner-most pads were fixed, and the other nine were allowed to move freely while optimizing for the D-array with a target resolution of just over $2''$ (a factor of $\sim 2.5$ lower than the C-array). After the D-array was created, the inner-most six pads of this array were fixed and again, the remaining nine were allowed to move within the star mask for the optimization with a target resolution of over $4''$ for the E array.

To create the B array, the outer-most five pads of the C array plus two inner ones were fixed, and the remaining eight pads were allowed to move within the constraint of achieving the target resolution of just over $0.3''$.

### 2.2. Notes on A-array

Creation of the A array was more difficult since the four western-most pads needed to be locked, since there is less geographical and sightline freedom on the western side of Rt 168. In addition to these pads, we locked five of the B array pads into place and allowed the code to optimize the remaining six pads with a target resolution of $0.15''$. The resulting array had some pads manually displaced from areas known to be geographically unsuitable.

The result of manually moving pads away from the optimal locations is that the maximum sidelobes are somewhat larger than they could be. We are unable to tweak the A array until we can better determine the geography of the desired pad locations. We are uncertain if the northern-most pad and southern-most 3 pads (east of Rt 168) are placed precisely on good pad locations. The pads just to the east of Rt 168 are as close to the ridge as is probably safe. Overlaying them on the site map and mask indicates that they may be OK to within $\sim$50 meters or so, but we cannot determine precise locations until we actually travel to the site in person again.

### 2.3. Notes on E-array

Our E-array has not been manually tweaked for packing and shadowing, and as a result it is heavily shadowed, and thus the beams are poorer at low declination. It is unlikely that we will be able to acheive the quality beams and shadowing features of the E array from Helfer & Wright (2003). If we adopt their E-array, we can reuse 4 of thier pads between their E and our D (compared to 7 reused pads for our E and D arrays together). So adopting the E-array from Helfer & Wright will result in us needing 3 more pads, bringing our total up to 53.

## 3. Results

Our beams are shown in Figures 3 and 4. The contour levels are -10, -5, 5, 10, 20, 40, 60, 80, 100%. Details of the beams and sidelobes are presented in Table 1. The sidelobe information in Table 1 is for the inner 14 × 14 beams only (as in Helfer & Wright (2003) and Helfer (2003). The sidelobe statistics for a larger area of 40 × 40 beams is presented in Table 2.

We set the target resolutions for each array to be similar to those of Helfer (2003), and the resulting scale resolution factors between arrays is between ∼2 and 2.5 (see Table 3).

### 3.1. Specific Cost Savings of the Star Array

1) Pad reuse: The star array uses 7 fewer pads than the purely optimized array (53 comapred to 60). This represents a 10% saving in pad construction and material costs.

2) Cable trenches: Straight cable runs will be simpler to build. They will require fewer pull stations (with easier pulls) and fewer connectors.

3) Roads: The star array will require fewer roads which saves initially on construction costs, and subsequently in maintainance and such issues as snow removal.

4) Operation: With all pads confined to single roads (except in A array) issues such as restarting drives after power failures is much simpler as you work along straight roads with less back tracking. Antennas with faults are simpler to find and reach in a hurry, especially to visiting observers who are unfamiliar with the site.

## 4. Important Notes on Comparing Configurations

We note that a few percentage differences in the peak sidelobes will most likely be undetectable in real observing conditions, with each dish having different system temperatures and occasionally being taken out of the array for mechanical faults. Testing shows that the rms value of the sidelobe percentage is rather robust to the removal of dishes from the array and observing source during non-transit conditions. The max and min sidelobe percent on the other hand can change by up to 5% of the peak intensity by simply observing from 0h to 4h LST instead of -2h to 2h, for example. This is true for both our star arrays and the purely optimized arrays of Helfer & Wright (2003) and Helfer (2003).

In our report, we present results in a similar fashion as Helfer & Wright (2003) for ease of comparison. We note that Table 1 only shows the sidelobe properties for the inner 14 × 14 beams (which corresponds to $2''$ in A array). To study the wide-field properties of the beams, in Table 2 we present the sidelobe parameters for the inner 40 × 40 beams which corresponds to $6''$ in A array and $90''$ in D array. The results for the 5-arm star are shown in in left columns of Table 2, while the arrays of Helfer & Wright (2003) are shown in the right columns. In almost all cases, the sidelobe properties are comparable.

Again, we note that our A-array has not been fine tuned to match the geography, so the peak sidelobes are higher than they likely will be in the final version.

## 5. Summary

We have generated a series of array configurations that have excellent beam properties and pad reusage. Construction of these arrays will be simplified since all roads and cable tunnels run along five straight arms. Given that all beams are generated assuming tracks $\pm 2$ hours over transit with all dishes operational and with equal system temperatures, the "real world" differences will not likely be enough to justify the increased cost of the purely optimal array over the optimized star array. Unfortunately, the work required to fit the star array onto Cedar Flats will likely cancel out much of the cost savings over the arrays of Helfer (2003).

G. R. P. is supported by NSF grant AST 99-81289 and by the State of Maryland via support of the Laboratory for Millimeter-Wave Astronomy.

## REFERENCES

Boone, F., 2001, A&A, 377, 368

Helfer, T., & Wright, M., 2003, CARMA Memo, *in prep.*

Helfer, T., 2003, CARMA Memo, *in prep.*

Table 1. Beam Parameters for the 5-Arm Star Arrays at 230 GHz

| Cfg | $\delta$ (°) | HA,inc (hrs) | $\sigma$ (mJy) | $\theta_{\mathrm{max}} \times \theta_{\mathrm{min}}$ ($''$) | $\sigma_{\mathrm{T_b}}$ mK | SL rms (%) | max (%) | min (%) | Nvis (%) | $uv$ min (m) | $uv$ max (m) |
|---|---|---|---|---|---|---|---|---|---|---|---|
| A | 30 | -2,2,.01 | 0.23 | 0.15 x 0.14 | 253.2 | 3.4 | 12.8 | -7.8 | 100 | 206.1 | 1792.5 |
| A | 0 | -2,2,.01 | 0.27 | 0.18 x 0.15 | 231.2 | 3.9 | 25.4 | -8.1 | 100 | 177.9 | 1792.5 |
| A | -30 | -2,2,.01 | 0.56 | 0.35 x 0.15 | 246.6 | 2.8 | 10.7 | -7.0 | 100 | 75.6 | 1792.5 |
| B | 30 | -2,2,.01 | 0.23 | 0.41 x 0.34 | 38.1 | 2.6 | 6.7 | -6.9 | 100 | 50.1 | 770.4 |
| B | 0 | -2,2,.01 | 0.27 | 0.42 x 0.41 | 36.3 | 3.2 | 13.6 | -7.2 | 100 | 36.6 | 739.2 |
| B | -30 | -2,2,.01 | 0.56 | 0.87 x 0.42 | 35.4 | 2.6 | 7.6 | -5.8 | 100 | 19.8 | 674.1 |
| C | 30 | -2,2,.01 | 0.23 | 0.99 x 0.86 | 6.2 | 2.5 | 7.7 | -5.9 | 100 | 26.4 | 296.1 |
| C | 0 | -2,2,.01 | 0.27 | 1.08 x 0.99 | 5.8 | 2.8 | 16.3 | -7.0 | 100 | 21.3 | 296.1 |
| C | -30 | -2,2,.01 | 0.56 | 2.14 x 1.03 | 5.9 | 2.1 | 6.0 | -5.8 | 100 | 12.6 | 295.5 |
| D | 30 | -2,2,.01 | 0.23 | 2.23 x 2.03 | 1.2 | 2.9 | 7.9 | -6.4 | 100 | 11.4 | 142.8 |
| D | 0 | -2,2,.01 | 0.29 | 2.49 x 2.04 | 1.3 | 3.6 | 12.7 | -7.6 | 87 | 9.3 | 138.0 |
| D | -30 | -2,2,.01 | 0.68 | 4.65 x 2.03 | 1.7 | 3.2 | 9.5 | -7.9 | 67 | 4.5 | 117.0 |
| E | 30 | -2,2,.01 | 0.23 | 4.17 x 3.82 | 0.3 | 2.7 | 7.1 | -7.3 | 99 | 8.7 | 63.3 |
| E | 0 | -2,2,.01 | 0.33 | 4.47 x 3.60 | 0.5 | 4.0 | 18.4 | -8.4 | 68 | 6.6 | 62.1 |
| E | -30 | -2,2,.01 | 1.07 | 7.68 x 3.10 | 1.0 | 4.9 | 21.0 | -11.8 | 26 | 3.0 | 62.1 |

Beam properties for the 5-arm star arrays shown in Figure 2. Column (1) is the array configuration; column (2) is the declination; column (3) is the LST range and step size of the observations; column (4) is the sensitivity (in mJy); column (5) beam size (in $''$); column (6) is the brightness temperature sensitivity (in mK). Columns (7),(8), and (9) are the sidelobe rms, max and min (respectively) over a $\sim 14 \times 14$ beam area. Column (10) is the percentage of unshadowed visibilities while columns (11) and (12) projected minimum and maximum baselines (in meters).

Table 2. Comparison of Sidelobe Parameters over 40x40 Beams for the 5-Arm Star and Helfer (2003)

| dec | Array | rms | max | min | Array | rms | max | min |
|---|---|---|---|---|---|---|---|---|
| 30 | star A | 2.5 | 12.8 | -7.8 | opt A | 2.3 | 8.7 | -7.0 |
| 0 | | 3.2 | 27.6 | -8.1 | | 2.8 | 19.0 | -7.1 |
| -30 | | 2.3 | 10.7 | -7.0 | | 2.2 | 8.8 | -6.7 |
| 30 | star B | 2.1 | 9.0 | -6.9 | opt B | 2.1 | 10.9 | -6.7 |
| 0 | | 2.9 | 26.5 | -7.2 | | 2.8 | 21.4 | -7.1 |
| -30 | | 2.1 | 10.7 | -5.8 | | 2.0 | 9.6 | -6.6 |
| 30 | star C | 2.2 | 11.6 | -5.9 | opt C | 2.1 | 8.4 | -5.9 |
| 0 | | 2.8 | 29.8 | -7.1 | | 2.8 | 27.6 | -6.9 |
| -30 | | 2.0 | 10.8 | -5.9 | | 2.0 | 7.9 | -6.2 |
| 30 | star D | 2.2 | 9.5 | -6.4 | opt D | 2.2 | 9.8 | -6.1 |
| 0 | | 3.4 | 30.5 | -7.6 | | 3.1 | 28.8 | -7.1 |
| -30 | | 2.5 | 9.5 | -7.9 | | 2.2 | 8.3 | -6.4 |
| 30 | star E | 2.1 | 8.0 | -7.3 | opt E | 2.1 | 8.8 | -6.7 |
| 0 | | 3.5 | 29.5 | -8.5 | | 3.0 | 21.2 | -7.1 |
| -30 | | 3.9 | 21.0 | -11.8 | | 4.0 | 18.3 | -11.3 |

Direct comparison of the sidelobe properties between the 5-arm star (left columns) and those of Helfer & Wright (2003) (labelled “opt A-E” in the right columns). We note that the maximum sidelobe is not a very robust measure of beam quality, and changes significantly with the removal of antennas from the array or variations in LST range over which the observations are taken. The “rms” sidelobe is more robust to small changes in observing parameters.

Table 3. Beam elongations, spatial dynamics ranges and SRFs at $\delta = 30°$

| Config | $\theta_{\rm max}$ ($''$) | $\theta_{\rm min}$ ($''$) | $\theta_{\rm max}/\theta_{\rm min}$ | $S_{\rm max}/S_{\rm min}$ | SRF |
|---|---|---|---|---|---|
| star A | 0.15 | 0.14 | 1.07 | 8.7 | |
| star B | 0.41 | 0.34 | 1.20 | 15.3 | B/A = 2.6 |
| star C | 0.99 | 0.86 | 1.15 | 11.2 | C/B = 2.5 |
| star D | 2.23 | 2.03 | 1.10 | 12.5 | D/C = 2.3 |
| star E | 4.17 | 3.82 | 1.09 | 7.3 | E/D = 1.9 |
| opt E | 4.48 | 3.94 | 1.14 | 8.8 | $\rm E_{opt}/D = 2.0$ |

Array beams and scale factors for the 5-arm star array. Column (1) is the array; columns (2) and (3) are the maximum and minumum beam elongation and column (4) is the ratio of the two. Column (5) is the ratio of maximum to minimum projected baseline and the last column is the Scale Resolution Factor between the average beam elongation of subsequent arrays. The last row shows the E array from Helfer & Wright (2003) and the scale factors achieved if we adopt this array into our configurations.

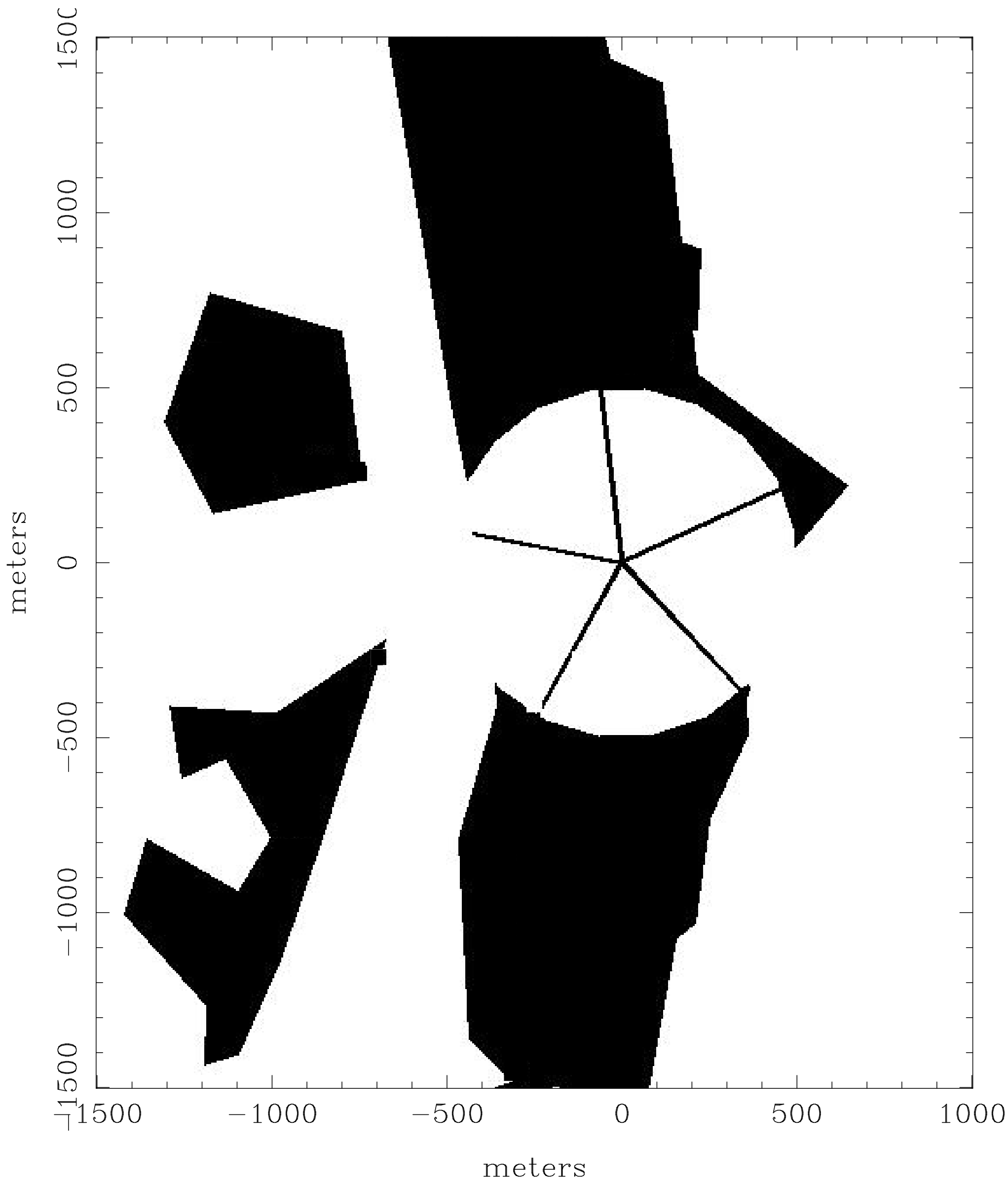


Fig. 1.— Shown is the mask used to generate the configurations shown in Fig 2. The arms are 500 m in radius and 10 m wide. The star orientation was choosen so that the large hill to the NE of the array center is between two arms. Also, it was important to try and keep only one arm crossing the ridge to the west of the array center (between the center and Rt 168).

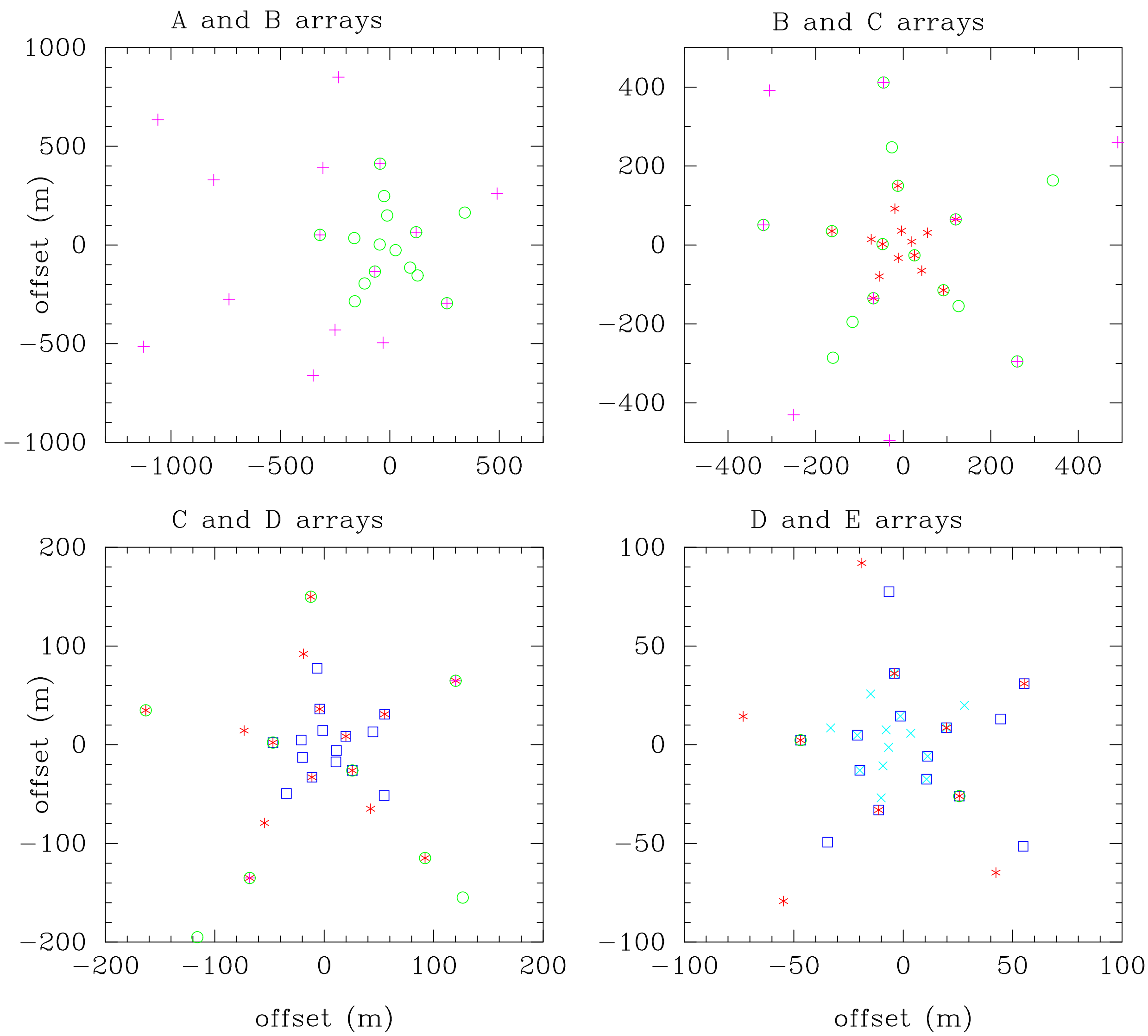


Fig. 2.— We zoom in on the arrays. The purple +'s mark the A array pads, the green circles mark the B array pads, the red *'s mark the C array pads, the blue squares mark the D array pads and the turquoise ×'s mark the E array pads. It is most likely that we will incorporate the superior E array of Helfer & Wright in place of our E-array. In this case we will need to add 3 more pads.

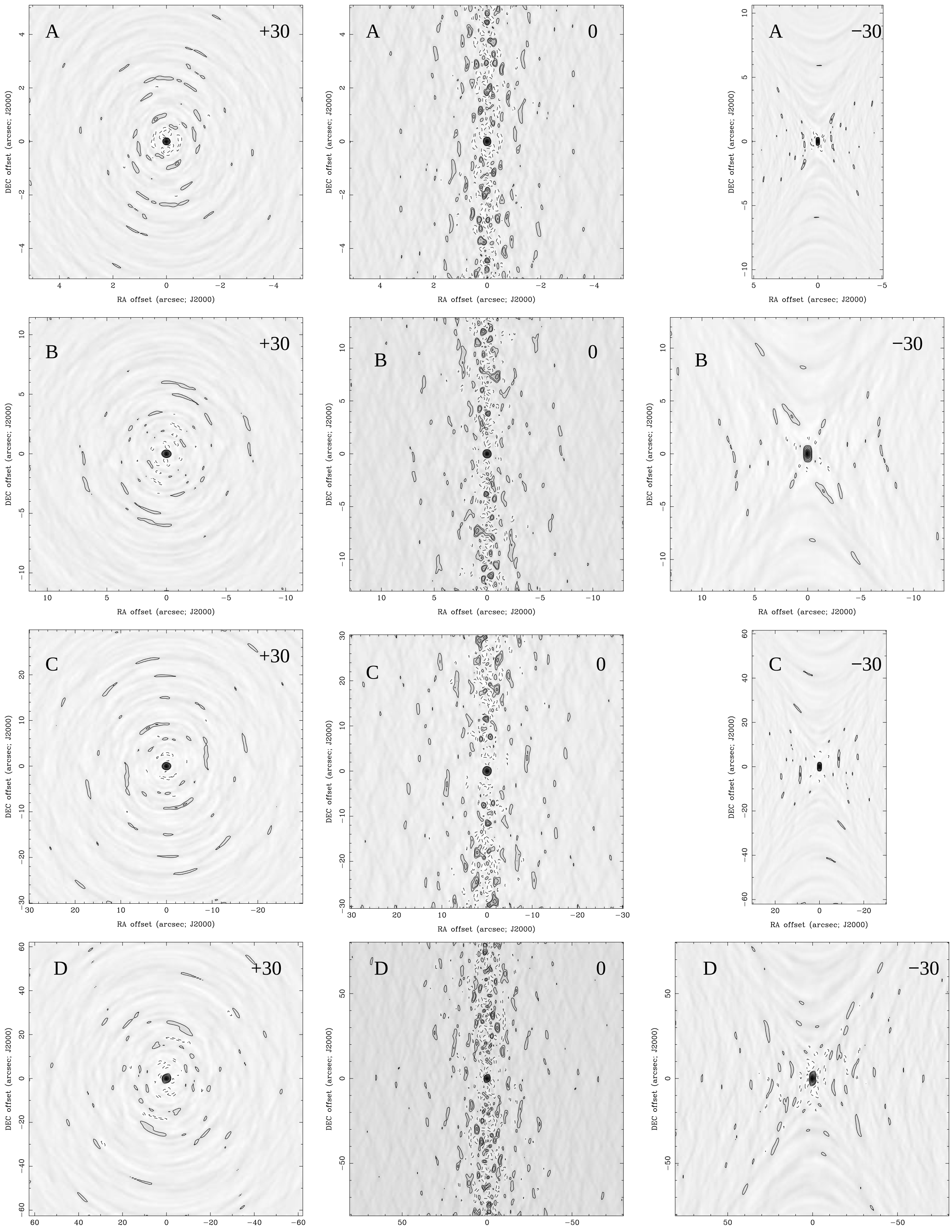


Fig. 3.— The resulting beams for the configurations shown in Figure 2. From top to bottom are the A, B, C, and D arrays respectively. From left to right we show beams for declinations of +30, 0, and -30 (respectively). The contour levels are -0.1, -0.05, 0.05, 0.1, 0.2, 0.4, 0.6, 0.8, 1.0 (fractions of the peak).

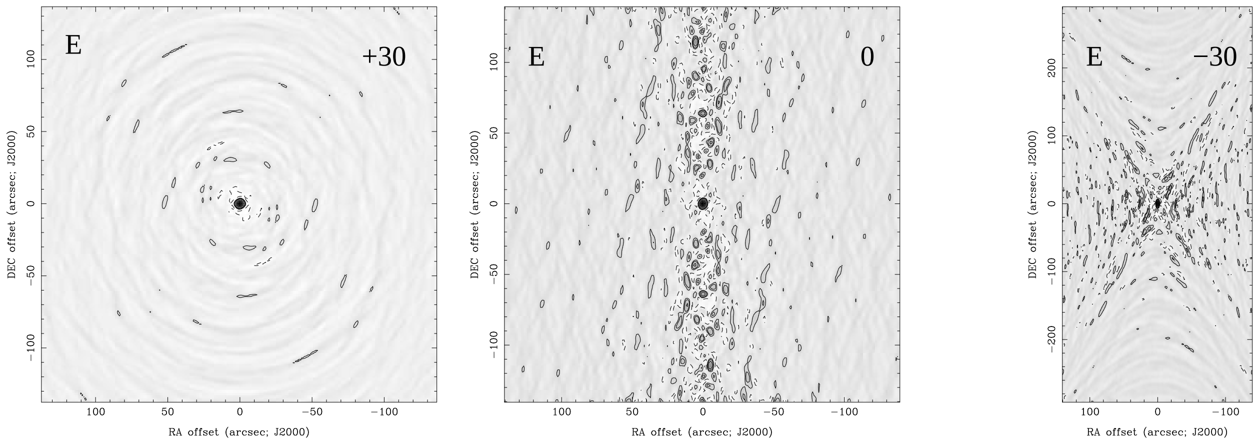


Fig. 4.— The resulting beams for the E configurations shown in Figure 2. From left to right we show beams for declinations of +30, 0, and -30 (respectively). The contour levels are -0.1, -0.05, 0.05, 0.1, 0.2, 0.4, 0.6, 0.8, 1.0 (fractions of the peak). It is not optimized for low dec sources and as a result is heavily shadowed. It is most likely that we will incorporate the superior E array of Helfer & Wright in place of our E-array.

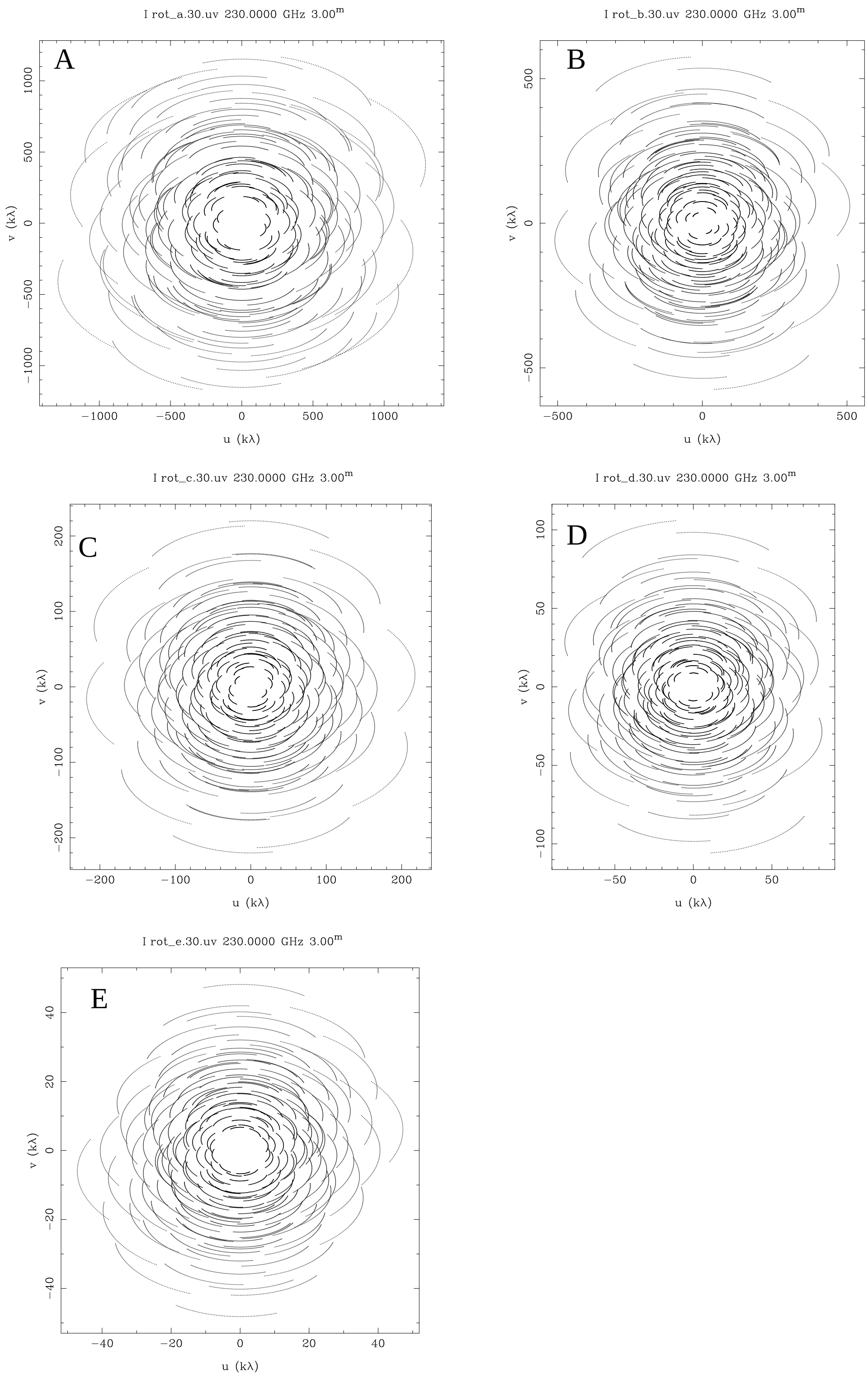


Fig. 5.— $uv$ plots for each of the configurations at a declination of $+30°$.

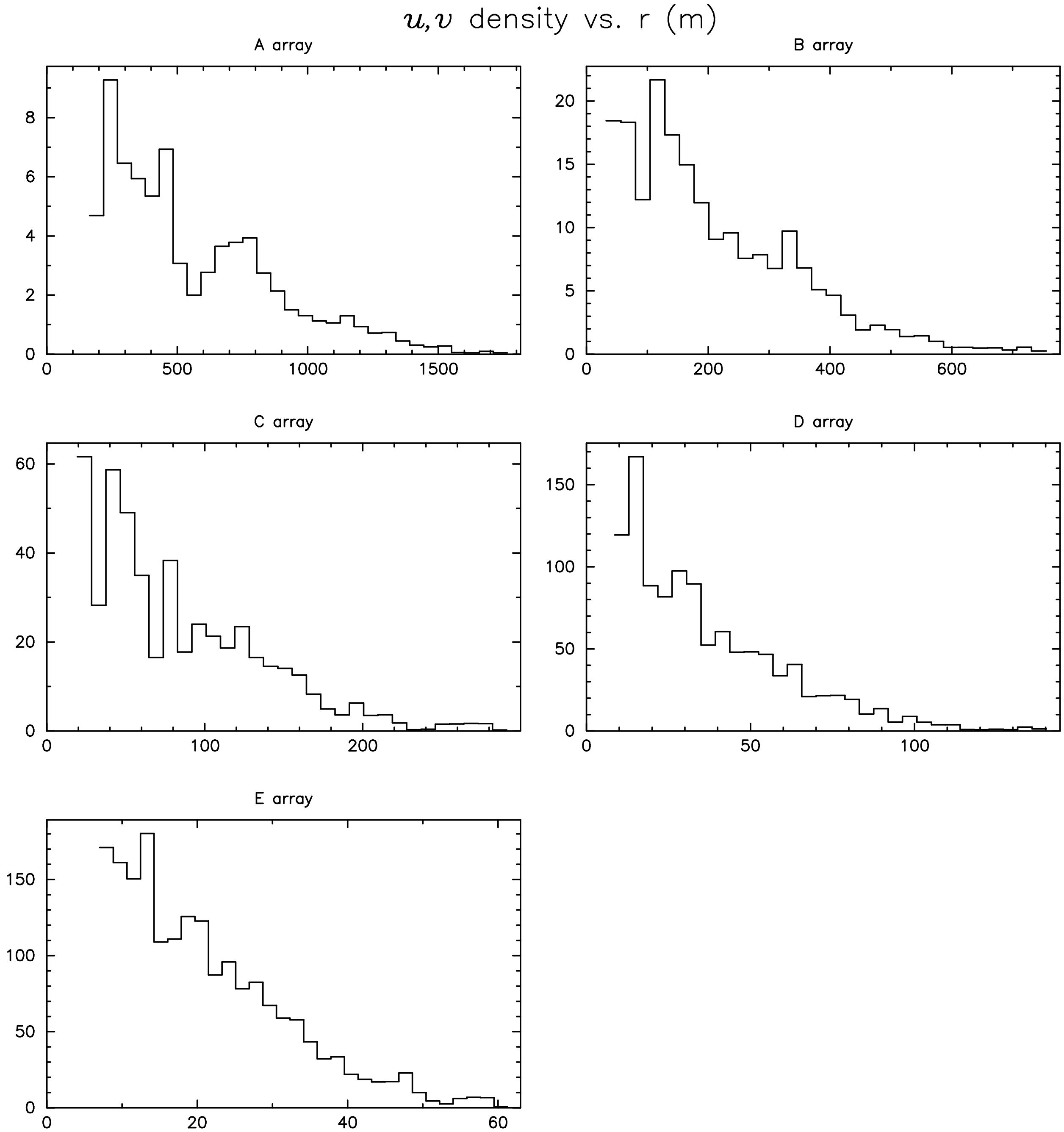


Fig. 6.— $uv$ density plots for each array showing the Gaussian distribution generated by the Boone code. What is not taken into account is the fact that the larger OVRO will weight some of these baselines differently, resulting in a slightly different (and perhaps non-optimal!) distribution than is shown here.